Liquid-crystal display of stress fields in ferroelectrics

Doru C. Lupascu,[a] Sergio L. dos Santos e Lucato, Jürgen Rödel
*Institute of Materials Science, Darmstadt University of Technology, Petersenstraße 23,
D-64287 Darmstadt, Germany*

Markus Kreuzer
*Institute of Applied Physics, Darmstadt University of Technology, Hochschulstraße 6, D-64289 Darmstadt,
Germany*

Christopher S. Lynch
*GWW School of Mechanical Engineering, The Georgia Institute of Technology, Atlanta,
Georgia 30332-0405*

Direct optical images of local surface potentials generated by the process zone of a crack are shown for a thickness-poled ferroelectric ceramic using liquid crystals. The observed potentials can be mapped to stresses within the material revealing the complex shape and time development of the process zone so far not accessible using other techniques. *© 2001 American Institute of Physics.*
[DOI: 10.1063/1.1365417]

In actuator applications,[1] ferroelectric ceramics frequently fracture under high electric fields or mechanical stresses,[2,3] constituting a major impediment to large-scale usage.[2] The fracture process is dominated by ferroelastic toughening,[4] which develops in a process zone around the crack tip.[5] Some of the external work is dissipated in the process zone partially shielding the crack tip from the singular applied stress field. Toughening by ferroelastic switching differs from dislocation motion in metals,[6] because it saturates, and from transformation toughening, because the ferroelastic domains can be reversibly reoriented.[6,7] Most importantly, the ferroelectric–ferroelastic switching couples to the electric field.[7] While brittle fracture of linear elastic materials[8] and toughening mechanisms in metals[6] or switch toughening ceramics[9] have been well modeled, the coupling of the ferroelectric–ferroelastic process zone to the electric field has so far not been sufficiently treated. The increase of fracture toughness with total crack length, the R curve, is known to be a function of the polarization state and the presence of electric field in ferroelectric ceramics,[5,10–12] but it has not been clear how much of this is due to a process zone with ferroelastic switching or due to the electric field inducing stress at the crack tip.[12]

This work explains how the piezoelectrically or ferroelectric–ferroelastically induced potential differences on the surface of a poled ferroelectric sample can be rendered optically visible and used to determine the complex elastic–anelastic stress field inside the material. This method offers a much more detailed insight into the processes at the crack tip than previously available. The results of the analysis are presented.

A thin layer of a nematic liquid crystal[13] is used to display the potential differences with respect to an optically transparent reference electrode (Fig. 1). A nematic liquid crystal consists of cigar-shaped molecules that tend to align parallel to each other without any ordering of their center of mass. For properly prepared surfaces of sample and electrode,[13] the long axes of the molecules are forced to align parallel to the surfaces and form via elastic coupling a bulk uniaxial birefringent layer. If potential drops occur normal to the external surfaces, the anisotropic polarizability induces a torque rotating the molecules and, therefore, the optical axis, into the direction of the electric field. For normal incident light, linearly polarized at 45° with respect to the in-plane orientation of the molecules, the effective birefringence is reduced and varies with voltage. Using a crossed analyzer, different voltages appear as colors in the reflected light given by the wavelength-dependent phase retardation between the ordinary and extraordinary waves. This first mode of operation is used with a free-floating potential at the reference electrode and allows us to monitor voltages in a wide range. Multiple sets of colors can be observed due to the large change of phase retardation.

In a second mode the orientation of the molecules is rotated by 45° between the two surfaces, yielding a smooth twist of the optical axis across the liquid-crystal thickness. Normal-incident light is linearly polarized at 0° with respect to the molecule orientation at the transparent electrode. Due to the waveguiding effect,[13] the polarization state remains linear during propagation through the sample and its polar-
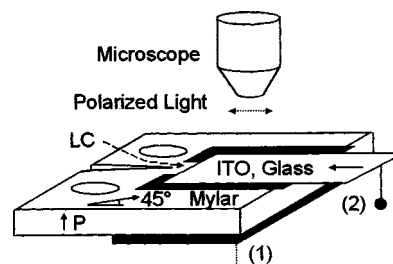

FIG. 1. Liquid-crystal display of the stress field in a ferroelectric compact tension specimen (see Ref. 14): (1) back electrode and (2) transparent electrode at fixed or floating potential. The arrows indicate the liquid-crystal orientation on each surface for the twisted nematic mode.

---

[a]Author to whom correspondence should be addressed; electronic mail:
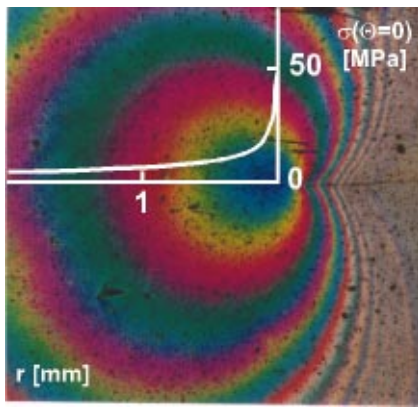lupascu@ceramics.tu-darmstadt.de

FIG. 2. (Color) Stress-generated electric potential contours prior to development of a plastic zone and crack advance in a poled ferroelectric compact tension specimen displayed by the floating potential mode. The crack tip is located at the origin of the inset. The elastic stress ahead of the crack is delineated ($K_I = 0.5$ MPa$\sqrt{m}$).

FIG. 3. (Color) Process zone potential field for a fully developed process zone before crack advance in the compensating twisted nematic mode.

ization direction follows the twist adiabatically. Independent of its wavelength, the polarization state of reflected light is not altered with respect to the incident light. The liquid crystal appears dark when viewed through a crossed analyzer. When subjected to an electric field, the molecules again tend to align parallel to the field. At low fields the twist angle remains almost uniform but undergoes a sharp transition at higher fields. The twist from 0° to 45° is confined to a thin layer in the middle of the sample.[13] At this transition, the polarization of the light can no longer follow the rapidly changing twist, resulting in a wavelength-dependent change of the polarization state. For the given conditions, the effective birefringence is low enough to yield a single set of color fringes. At very high fields all molecules are aligned parallel to the field, and the sample appears dark again. The edge of fringes represents a well-defined potential difference. The reference potential can now be externally varied and the values of the surface potentials scanned as two-dimensional (2D) optical images of well-determined equal potential (compensating voltage twisted nematic mode).

The ferroelectric sample is a compact tension specimen[14] ($50 \times 48 \times 3$ mm^3) of a commercial soft Ni/Sb co-doped PZT at the morphotropic phase boundary[10] (PIC 151, Lederhose, Germany) poled in the thickness direction. The liquid-crystal layer of thickness 23 μm is constituted of the nematic mixture ZLI-3086 (Merck KGaA, Darmstadt) exhibiting dielectric anisotropy $\Delta\varepsilon = 0.1$, specific resistivity $\rho > 5 \times 10^{14}$ Ωcm, and birefringence $\Delta n = n_e - n_o = 0.1131$. The planar alignment at the surfaces was achieved by spin coating a polyimide layer (Kit ZLI 2650, Merck) and subsequent unidirectional rubbing. A voltage of 45 V suffices to fully rotate the liquid crystal out of plane. Compensating voltages range from 0 to 1000 V. The transparent electrode is commercial Sn:In$_2$O$_3$ on glass.

The surface potentials are optically visible on the entire sample surface in any stage of loading, crack propagation, and unloading. At low loads only the elastically applied stress field is seen (Fig. 2). The in-plane principal stresses σ_1 and σ_2 yield the out-of-plane piezoelectric response of the ferroelectric via the piezoelectric charge constant $E_3 = g_{31}$ ($\sigma_1 + \sigma_2$). Figure 2 shows contours of equal potential in the floating potential mode. For higher loading, a circular pro-
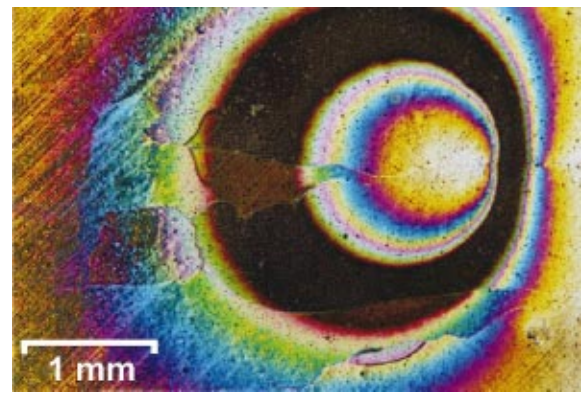
cess zone develops in front of the crack tip. Figure 3 displays the almost circular inner (positive) and outer (negative) contours of the equal potential drop within the process zone just before crack advance in compensating mode for a particular compensating voltage. For an advancing crack, part of the process zone also becomes located along the crack faces, modifying the elastic stress field even at locations remote from the crack tip. Figure 4, in compensating mode, shows the circular contours of the equal potential ahead of the crack tip (a), the process zone, and modifications of the elastic stress field due to it in the crack wake (b) and the width of the residual plastic deformation of material after the crack tip has well passed this region (c). The process zone is wider near the crack tip and relaxes to a smaller size of remnant deformation (c). The whole complexity of such stress fields is apparent.

For a quantitative analysis, the backside of the ferroelectric is electroded and grounded [(1) in Fig. 1]. The compensating potential is externally varied. The fringes extend or contract according to the voltage applied. For each voltage, a complete 2D contour of equal potential is given by the fringe edge and can be quantified, e.g., along the radial ray straight ahead of the crack (inset, Fig. 2). The surface potentials as a function of radial distance from the crack tip are shown in Fig. 5. The induced potential reflects the accumulation of the piezoelectric effect due to planar stresses throughout the total thickness. Far from the crack tip, the applied stress can
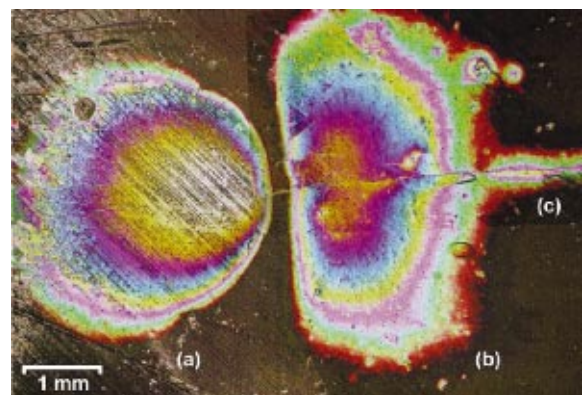

FIG. 4. (Color) (a) Elastic–plastic stress field ahead of the crack tip, (b) modification of the elastic stress field due to the process zone, and (c) the remnant polarization of the process zone outside the elastic stress field of the crack tip in the quantitative compensating twisted nematic mode.
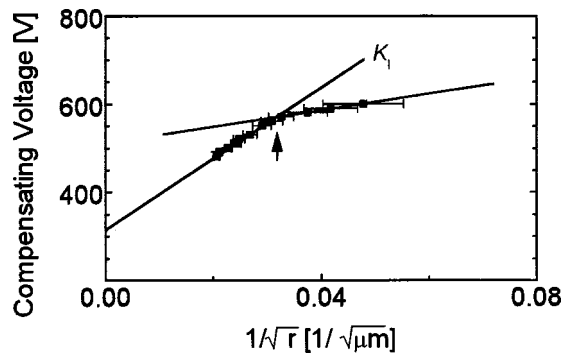
FIG. 5. Electric potential ahead of the crack tip plotted vs $1/\sqrt{r}$ for a 30-mm-long crack at a crack intensity of $K_I = 1.6\,\mathrm{MPa}\sqrt{m}$ after 4.4 mm crack advance at crack velocity 10^{-5} m/s.

readily be computed from handbook solutions.[15] From a comparison of the far-field applied stress (25 MPa at the crack length of 30 mm) and measured electric potential away from the crack tip, an effective charge constant $g_{31} = 0.004\,09$ Vm/N is obtained. The dominating term of the singular stress field around the tip (in excess of the applied stress) is generally written as

$$\sigma_y(\Theta = 0) = \frac{K_I}{\sqrt{2\pi r}}.$$

Using the piezoelectric coefficient g_{31} as obtained above, the elastic part of the crack tip stress field can be obtained yielding a stress intensity factor of $K_I = 1.6\,\mathrm{MPa}\sqrt{m}$, consistent with the value obtained from crack length and applied load (Fig. 5). Closer to the crack tip, but still far away with respect to previous approximations of process zone size, partial anelastic deformation is seen and the potentials/stresses drop beneath the elastic limit. The transition point is marked by an arrow (Fig. 5, edge at 1.2 mm from the crack tip). Even within the anelastic zone, a $1/\sqrt{r}$ dependence develops. This is a combined effect of reduced stress and the simultaneously reduced piezoelectric constant in the process zone.

Different types of time-dependent relaxation of the 2D stress field can also be observed. These include a growing

plastic zone at fixed stress intensity, relaxation (time-dependent reversal of domain switching) ahead of the crack tip after complete unloading, and relaxation of the very near-tip region ($<150\,\mu$m) upon external potential changes. After fast unloading, the size of the initial anelastic process zone relaxes with a time constant of $\tau = 260$ s $[K(t) = K(t = 0)\exp(-t/\tau)]$. This time constant is consistent with previous R-curve results where relaxation in the range of minutes[5] was reported.

The liquid-crystal method allows access to the stress fields around a crack in a poled ferroelectric. A precise and quantitative analysis of such data in future work promises to fully reveal the process zone behavior and time-dependent effects.

[1] G. H. Haertling, J. Am. Ceram. Soc. **82**, 797 (1999).
[2] K. Uchino, *Piezoelectric Actuators and Ultrasonic Motors* (Kluwer Academic, Boston, MA, 1997).
[3] G. A. Schneider, A. Rostek, B. Zickgraf, and F. Aldinger, in *Crack Growth in Ferroelectric Ceramics under Mechanical and Electrical Loading*, Electroceramics IV, edited by R. Waser *et al.* (Augustinus Buchhandlung, Aachen, Germany, 1994), pp. 1211–1216.
[4] K. Mehta and A. V. Virkar, J. Am. Ceram. Soc. **73**, 567 (1990).
[5] F. Meschke, O. Raddatz, A. Kollek, and G. A. Schneider, J. Am. Ceram. Soc. **83**, 353 (2000).
[6] T. L. Anderson, *Fracture Mechanics* (CRC, Boca Raton, FL, 1995).
[7] B. Jaffe, W. R. Cook, Jr., and H. Jaffe, *Piezoelectric Ceramics* (Academic, Marietta, OH, 1971).
[8] B. Lawn, *Fracture of Brittle Solids* (Cambridge University Press, Cambridge, U.K., 1975).
[9] A. G. Evans and A. H. Heuer, J. Am. Ceram. Soc. **63**, 241 (1980).
[10] S. L. S. Lucato, D. C. Lupascu, and J. Rödel, J. Am. Ceram. Soc. **83**, 424 (2000).
[11] G. A. Schneider and V. Heyer, J. Eur. Ceram. Soc. **19**, 1299 (1999).
[12] C. S. Lynch, W. Yang, L. Collier, Z. Suo, and R. M. McMeeking, Ferroelectrics **166**, 11 (1995).
[13] P. Yeh and C. Gu, *Optics of Liquid Crystal Displays* (Wiley, New York, 1999).
[14] ASTM Standard E 1820-96, *Annual Book of ASTM Standards* (American Society for Testing Materials West Conshohocken, PA, 1997), Vol. 03.01.
[15] H. Tada, P. Paris, and G. Irwin, *The Stress Analysis of Cracks Handbook* (Paris, St. Louis, MO, 1985).